

MICRO-SCALE ASPECTS OF CHEMICAL-MECHANICAL COUPLING: INTERPARTICLE FORCES AND FABRIC

J.C. Santamarina

Georgia Institute of Technology, Atlanta, Georgia, USA

K.A. Klein

University of Toronto, Toronto, Canada

A. Palomino and M.S. Guimaraes

Georgia Institute of Technology, Atlanta, Georgia, USA

ABSTRACT: Mineralogy and pore fluid determine the chemical-electrical characteristics on mineral surfaces, the ensuing interparticle electrical forces, fabric formation and its potential alteration during pore fluid changes. The region in the particle size vs. stress space where chemical-mechanical coupling may take place reflects the relevance of double layer phenomena and the relative balance between local contact-level electrical forces and boundary-skeletal forces resulting from Terzaghi's effective stress. Analytical results show that significant chemical-mechanical coupling can be expected in fine-grained soils (e.g., clays) at low confinement. Fabric formation/alteration in clay minerals is complex; in its simplest form, it can be captured in the pH-concentration space. Chemical-mechanical coupling may lead to unforeseen results because of the complexity of clay fabric formation and the interaction between multiple internal scales. While heuristically modified effective stress principles can be used to model some observed results in chemical-mechanical coupling, they are physically ill-posed, and fail to predict important aspects of the observed response.

1 INTRODUCTION

Energy coupling phenomena can be supported on the bases of fundamental physical principles including energy conservation and Le Châtelier's principle. The principle of energy conservation postulates that energy can be transformed from one form to another, and transferred from one body to another, but the total amount of energy in the system remains constant. Le Châtelier's Principle states that a system in equilibrium will oppose any disturbance (Holden, 1965; Ikeda, 1990). Energy coupling develops not only under steady state conditions (Mitchell, 1993), but in dynamic events as well (Santamarina and Fratta, 2001).

Chemical-mechanical coupling in soils refers to the change in mechanical properties in a medium subjected to chemical changes; the counter effect also takes place. The effects of chemical-mechanical coupling can be relevant in fields such as geo-environmental applications (e.g., fracturing of clay liners, implications of contaminant migration), petroleum exploration and production (e.g., stability of shales and chalk), as well as other fields that involve porous media, such as bioengineering.

The purpose of this paper is to identify the governing micro-scale mechanisms that control chemical-mechanical energy coupling in soils. The study

starts with an evaluation of interparticle forces to identify the region of interest to chemical-mechanical energy coupling. Then, published results are carefully analyzed to assemble the map of particle interaction and fabric formation in clay minerals. Finally, multi-scale aspects of chemical-mechanical coupling are discussed.

2 INTERPARTICLE FORCES - THE DOMAIN OF ENERGY COUPLING

Particles in a saturated granular medium are subjected to both skeletal and contact-level electrical forces. The electrical forces, when the interparticle distance exceeds $\sim 20 \text{ \AA}$, combine osmotic repulsion with electrostatic and van der Waals attraction; at shorter distances, oscillatory hydration forces manifest and when particles come into direct contact, Born repulsion takes over preventing interpenetration.

Expressions to estimate the order of magnitude of these forces are presented next (details can be found in Santamarina, Klein and Fam, 2001). For convenience, it is assumed that particles are circular discs, parallel to each other at a separation t greater than $\sim 20 \text{ \AA}$,

Skeletal force $F_{sk} = d^2 \sigma'$ (1)

$$\text{Attraction} \quad F_{\text{Att}} = \frac{1}{24} \frac{A_h}{t^3} d^2 \quad (2)$$

$$\text{Repulsion} \quad F_{\text{DL}} = 16\pi RT c_o d^2 e^{-\frac{t}{\vartheta}} \quad \text{large } t \quad (3a)$$

$$F_{\text{DL}} = \frac{1}{2} \pi RT c_o d^2 \left(\frac{2\pi^2 \vartheta^2}{t^2} - 1 \right) \quad \text{small } t \quad (3b)$$

The parameters in these equations are: particle diameter d , separation distance between particles t , bulk fluid ionic concentration c_o , applied effective stress σ' , Hamaker constant A_h ($A_h=0.64 \cdot 10^{-20} \text{J}$ for silica-water-silica and $A_h=0.09 \cdot 10^{-20} \text{J}$ for silica- CCl_4 -silica), gas constant $R=8.314 \text{ J}/(\text{mol}\cdot\text{K})$, absolute temperature T , Debye-Hückel length or double layer thickness ϑ (presented later in the text), and unit weight of the mineral that makes the particle γ_s . As a reference, the weight of a disk in terms of the particle slenderness α =diameter/thickness, is

$$\text{Weight of a disk} \quad W = \frac{\pi}{4} \frac{\gamma_s}{\alpha g} d^3 \quad (4)$$

Equations 1 through 4 can be rewritten in terms of macro-scale parameters by making the following two substitutions. First, the separation distance t between disks is expressed in terms of the water content w , the specific surface of the particles S_a , gravity g , and the unit weight of water γ_w as $t=2gw/(S_a\gamma_w)$. Second, the diameter of the particle d is related to the specific surface and the slenderness of the particle α , $d=(2\alpha+4)g/(S_a\gamma_s)$.

These relations can be used to predict the chemical-mechanical strain experienced in a soil during the propagation of an ionic concentration front. Consider platy particles stacked parallel to each other with adsorbed layers in between, and in equilibrium with the applied constant normal stress σ . The strain experienced by the stack of discs due to the change in chemical concentration Δc_o reflects the change in the pore fluid thickness (Figure 1 - insert). The following simplified expression is obtained for a small concentration change Δc (second order Taylor expansion), taking into consideration the repulsion force only (Equation 3b),

$$\varepsilon = \frac{t_f - t_o}{L_s + t_o} \approx \frac{\pi T^2 R^2 \gamma_s \sqrt{\frac{\varepsilon}{2}}}{g F z} \frac{S_a \Delta c}{(\sigma + 2RTc_o)^{3/2}} \quad (5)$$

where L_s is the particle thickness and c_o is the initial concentration in the bulk fluid. This equation predicts higher strains when the initial stress and concentration are low, and the specific surface of the soil is high (i.e., small particles). The strain is proportional to the change in concentration.

Figure 1 shows iso-strain contour lines as a function of the applied stress and the specific surface of

the soil. The figure was computed taking into consideration repulsion and attraction forces (Equations 2 and 3a&b), for an initial concentration $c_o=10^{-4} \text{ mol/L}$ (similar to fresh water) and a final concentration $c_f=0.4 \text{ mol/L}$ (similar to sea water). Results show that chemical-mechanical coupling is most significant in high specific surface soils subjected to low confining stress. Experimental data obtained for montmorillonite by di Maio (1996), and gathered by Santamarina and Fam (1995) for silica flour, kaolinite and bentonite are superimposed on the figure. (Note: SiO_2 grain surfaces in silica flour develop pH and concentration dependent surface charges - see Parks, 1990 - this is similar to clays, albeit the surface charge densities are more modest in quartz.) It is important to highlight that such a simple micro-scale analysis at the particle level can capture, at least on the order of magnitude, the relevance of chemical-mechanical coupling in different soils.

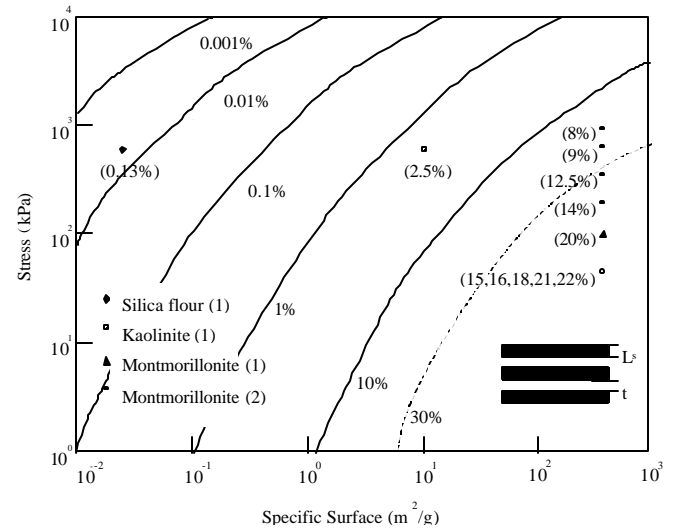


Figure 1. The effects of specific surface and initial state of stress on chemical-mechanical coupling - selected iso-strain lines are presented. The analysis presumes parallel platy particles. The following model parameters are assumed: initial concentration $c_o=10^{-4} \text{ mol/L}$ (similar to fresh water), final concentration $c_f=0.4 \text{ mol/L}$ (similar to sea water), valence of the prevailing ions $z=1$, and Hamaker constant $A_h=6 \cdot 10^{-20} \text{ J}$. Experimental data (1) from Santamarina and Fam (1995) and (2) de Maio (1996).

3 CLAYS AND FABRIC

The region for chemical-mechanical coupling identified above highlights the relevance of submicron particles in this phenomenon. Clays prevail in this size range, therefore, special emphasis is placed on identifying phenomena relevant to clay minerals.

Clay minerals are phyllosilicates, which are structures made of sheets with at least one of those sheets being silica. The building block of the silica sheet is the Si-tetrahedron, which consists of Si^{4+} at the cen-

tre of a tetrahedron with O^{2-} at the vertices. The other clay forming sheets are octahedral-shaped with OH^- at the vertices and either Al^{3+} or Mg^{2+} inside, rendering gibbsite and brucite, respectively.

The stacking of the sheets determines the type of clay mineral (Weaver, 1989; Mitchell, 1993). Kaolinite is a 1:1 stacking of gibbsite and silica; therefore, kaolinite presents OH^- termination sites on the gibbsite face, O^{2-} termination sites on the silica face, and both OH^- and O^{2-} termination sites on the edges (Figure 2). Layers made of 2:1 stacks of sheets involve silica-gibbsite-silica or silica-brucite-silica; two such layers can be linked through cations and/or water molecules resulting in clay minerals such as illite, montmorillonite and chlorite. Therefore, both faces in 2:1 clay minerals are silica and present O^{2-} termination sites, while the edges have both OH^- and O^{2-} termination sites (Figure 2).

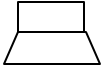
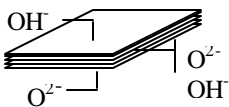
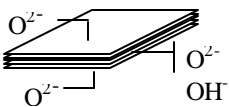
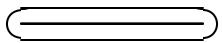
	1:1 Minerals Kaolinite	2:1 Minerals Montmorillonite
Mineral structure	 octahedral tetrahedral	 tetrahedral octahedral tetrahedral
Termination sites on particle faces and edges		
Particle size and adsorbed layers	$L = 1-20 \mu m$ Thickness $t \approx L/30$ Adsorbed layer thickness 100 \AA  <i>Adsorbed layer plots thinner than the trace used for the edge</i>	$L < 100t < 0.1 \mu m$ Thickness $t \approx 9.6 \text{ \AA}$ Adsorbed layer thickness 100 \AA 

Figure 2. The structure of clay minerals, edge and face termination sites, particle size, and adsorbed layers. The double layer created by the face may hide the local conditions around the edge in very thin particles such as a fully swollen montmorillonite. This is not the case in thick particles such as kaolinite.

Due to the structure of clay minerals, clay behavior is controlled by particle-fluid and particle-particle interactions. A comprehensive review of published results is presented next. The goal is to unravel fabric formation/alteration in fine grained minerals.

3.1 Particle-fluid interactions

The clay particle has "structural charge". Oxygens O^{2-} in Si-tetrahedral units and hydroxyls OH^- in octahedral units are shared with neighbors, rendering an electrically neutral structure in infinitely long sheets. However, the existence of lateral boundaries on the sheets implies uncompensated charges. In addition, isomorphic substitution of higher valence ions with lower valence ions, while preserving the structure of the sheets, renders additional negative charge during the formation of the mineral (e.g., Si^{4+} with Al^{3+} in Si-tetrahedra or Al^{3+} with Mg^{2+} in Al-octahedra). Structural disorder and defects may also contribute to the particle charge.

When dry, the neutralizing counterions are tightly bound to the surface of the particle, and excess ions form salt precipitates. When wet, precipitated salts hydrate and form the bulk fluid electrolyte with concentration c_0 , while the counterions on the particle surface hydrate and tend to move away from the particle surface (the combined effects of water polarity and the diffusing effects of thermal agitation). However, the attraction force between the counterions and the charged surface restricts the movement of the counterions. The competing effects of thermal agitation and electrostatic forces result in a characteristic concentration distribution: for negatively charged minerals, there is a high cation and low anion concentrations near the particle, reaching bulk fluid concentrations with distance from the surface. A layer of tightly bound ions remains near the surface (Stern layer) and a region of diffuse ions follows (Gouy layer). The Stern layer is a few angstroms in thickness and the boundary between the two layers is called the outer Helmholtz plane (Lyklema, 1995). This structure is summarized in Figure 3. The boundary between the Gouy layer and the bulk fluid is fuzzy due to the random movements of hydrated cations and anions. The thickness of the diffuse double layer, or the characteristic Debye-Hückel length, ϑ is taken to be the distance at which the potential decays to $1/e$ of the Stern potential ψ_{stern} , and it is equal to

$$\vartheta = \left(\frac{\epsilon' k T}{2c_0 e_0^2 z^2 N_{av}} \right)^{1/2} = \left(\frac{\epsilon' R T}{2c_0 z^2 F^2} \right)^{1/2} \quad (6)$$

where T is absolute temperature [K], c_0 is the ionic concentration in the bulk solution [mol/m^3], ϵ' is the real permittivity of the solution [farad/m], and z is the valence of the prevailing cation. The constants invoked are the elementary charge ($e_0 = 1.602 \cdot 10^{-19}$ C), Boltzmann's constant ($k = 1.38 \cdot 10^{-23}$ J/K), Avogadro's number ($N_{av} = 6.022 \cdot 10^{23}$ mol^{-1}), the gas constant ($R = 8.3145$ J/mol·K), and Faraday's constant ($F = 96485.3$ C/mol).

3.2 The effects of pH and concentration - Particle charge and dissolution

The characteristics of the pore fluid (in particular its pH, ion type and concentration) affect not only the effective charge on the mineral surface, but they

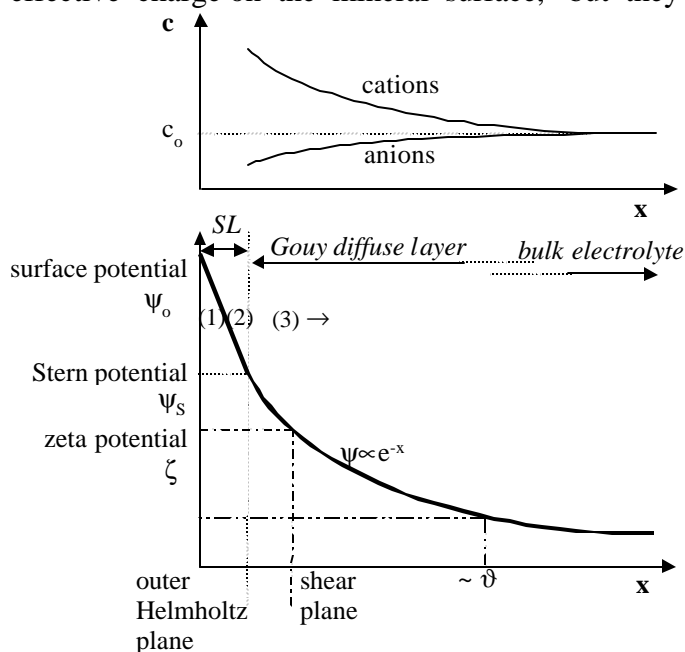


Figure 3. Ionic distribution and variation in electrical potential adjacent to a negatively charged particle. (1) inner sphere complexes, (2) outer sphere complexes, (3) diffuse ion swarm, SL = Stern layer, δ = double layer thickness. (Note: the common assumption of $\psi_{st} \approx \zeta$ is questionable).

may also promote the dissolution of the mineral. In fact, the charge of a particle is not necessarily an inherent quantity, but it depends on the adopted definition, which relates to the measurement method.

Structural Charge σ_0 . The structural charge, which results from uncompensated charges at boundaries and isomorphous substitution, is quite stable. It can be affected by mineral dissolution and by ionic diffusion within the solid phase (diffusion is very slow).

Adsorbed Protons (σ_H) and Ions (Δq). The structural charge σ_0 is compensated by adsorbed charges. Adsorption is controlled by the affinity of a species for the particle and by the abundance of the charges. Species that are constituents of the particle preferentially associate with it. Therefore, OH^- and H^+ (H_3O^+) are favored in oxides and are often called "charge or potential determining ions". Protonation is the adsorption of protons H^+ at termination sites, therefore, protonation adds positive charge to the particle ($\text{M-OH}^- + \text{H}^+ \leftrightarrow \text{M-HOH}$, where M represents a metal). On the other hand, an abundance of OH^- ions promotes the removal of protons from OH^- termination sites to form water ("deprotonation"), increasing the negative charge of the particle ($\text{M-OH}^- + \text{OH}^- \leftrightarrow \text{M-O}^{2-} + \text{H}_2\text{O}$; Lyklema, 1995; Stumm, 1992). The role of OH^- and H^+ is most important on the octahedral

face of 1:1 minerals (e.g., gibbsite face of kaolinite) and on the OH^- termination sites on the edges of both 1:1 and 2:1 clay minerals (Figure 2). Should all OH^- termination sites become protonated, the particle charge could exceed 3 to 4 C/m^2 . However, more modest charge densities are inferred from experimental data. Thus, the extent of protonation not only reflects the availability of OH^- surface sites, but also indicates the balance of Coulombian repulsion between protons, the effect of the local electrical field and the diffusing effects of thermal agitation.

Other ions besides OH^- and H^+ may be adsorbed on the particle surface forming inner sphere complexes (ions that have lost all or part of their primary hydration shell, thus there are no water molecules between the particle and the adsorbed element), outer sphere complexes (ions that retain their primary hydration shell), and the swarm of hydrated ions in the diffuse layer. Cation adsorption is the prevailing mechanism altering the charge of surfaces with O^{2-} termination sites, such as on silica faces (the basal plane of a Si-sheet has an O^{2-} termination site every 4.8 \AA^2). A slight increase in ionic concentration causes the Stern potential to become less negative. As concentration continues to increase, cation adsorption may render the particle neutral or even positively charged. Small, high-valence cations are the most efficient at modifying surface charge, thus explaining the effectiveness of Al^{3+} ions (see Amiratharajah and Mills, 1982; Lovgren et al., 1990). Indeed, monovalent ions would require a high surface density, which would be opposed by inter-ion Coulombian repulsion. (Cation complexation reactions are discussed in Hayes and Leckie, 1987. Inner sphere complexation of cations in the hexagonal cavities between O^{2-} on the basal plane of the Si-sheet has been experimentally verified by Nishimura et al., 1994.) Cation complexation can also take place near OH^- surface sites. Therefore, protonation and cation complexation are not independent processes.

Charge Balance. The strength of Coulombian forces requires that the particle and its adsorbed ions satisfy electroneutrality. Therefore,

$$\sigma_0 + (\sigma_H + \Delta q) = 0 \quad (7)$$

pH and Concentration. The abundance of H^+ ions is measured in terms of pH, while the abundance of other ions is specified in terms of ionic concentration c [mol/L]. Consequently, protonation and cation complexation must be studied in terms of the pH and the concentration c_0 of the pore fluid. The interplay between protonation and cation complexation is readily demonstrated by changing the ionic concentration of a suspension while monitoring the change in pH, as shown in Table 1 for a kaolinite-NaCl mix-

ture (see related experimental results in Williams and Williams, 1978).

Alternative Definitions of Particle Charge. Different test procedures gain access to different levels of the adsorbed layers surrounding the particle. Two definitions central to the analysis of fabric formation follow (Sposito, 1998):

- Point of Zero Charge (PZC) is the pH value when the diffuse charge is zero, $\sigma_o + \sigma_H + \sigma_{\text{Stern}} = 0$ (in this

Table 1. Value of pH reached in kaolinite suspensions in NaCl solutions of different concentration (Klein, 1999)

concentration [mol/L]	pH
$1 \cdot 10^{-5}$	6.01
$4 \cdot 10^{-4}$	5.20
$3 \cdot 10^{-3}$	4.58
0.1	3.95
1.8	3.82

case, the Stern potential is zero, $\psi_{\text{Stern}} = 0$). It is often associated with the pH at which a suspension coagulates rapidly (this may not be the case in thick particles such as kaolinite, because edge-to-face flocculation may develop when the isoelectric point of the particle edge is reached, as discussed later).

- Particle Isoelectric Point (IEP) is the value of pH when the electrophoretic mobility of the particle is zero, in other words, when the charge of the particle and its surroundings enclosed by the shear plane is zero. In this case, the ζ -potential = 0. (Electrophoretic mobility is measured by subjecting a dilute suspension to an electric field. The ζ -potential for a given measured mobility is computed using the Smoluchowski formula.)

The PZC and the IEP reflect the balance between different charges (Figure 3), and in general render different pH values. These differences reflect the entrapment of diffuse ions within the shear plane and the effects of particle geometry on mobility-related phenomena.

It follows from the discussion of protonation and cation complexation that the PZC and IEP vary with the availability of OH⁻ termination sites (clay mineral), and the ionic concentration and valence of prevailing ions in the fluid (Table 2).

Table 2. Isoelectric Points (IEP) for Kaolinite and Montmorillonite

concentration [mol/L]	electrolyte	part/face IEP	edge IEP
Kaolinite (1)			
10^{-4}	NaCl	3.9	
10^{-3}	NaCl	<3	
10^{-2} to 10^{-4}	NaCl		7.2
Montmorillonite (2)			
$10^{-5.5}$ to 10^{-1}	NaCl	N	*

$10^{-5.5}$ to 10^{-1}	Ca(NO ₃) ₂	N	*
$10^{-4.7}$	Th(NO ₃) ₂	3	*
$10^{-3.8}$	Al(NO ₃) ₂	4	*

* The edge IEP for montmorillonite is difficult to obtain due to the overwhelming impact of the face double layer.

N No particle (face) IEP was evident. For the given electrolyte and ionic concentration, the ζ -potential was negative at all pH.

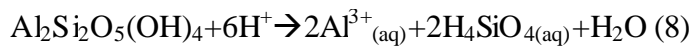
(1) from Williams and Williams (1978)

(2) from Delgado et al. (1986)

Experimental data show that the ζ -potential is more negative at high pH, low ionic concentration and low ion valence; however the ζ -potential becomes more positive with the increased availability of OH⁻ termination sites for possible protonation. While kaolinite (1:1 clay) has OH⁻ termination sites on the gibbsite face as well as on the edges, montmorillonite and mica (2:1 clays) have exposed OH⁻ sites only on the edges. Thus, the ζ -potential of 2:1 minerals is less sensitive to pH than 1:1 minerals. In fact, an IEP may not be found in 2:1 clays at low ionic concentrations of low valence electrolytes (Nishimura et al., 1992). However, an IEP may be found at low concentrations for higher valence electrolytes (Delgado et al., 1986 - Table 2).

Edge and Face Charge. The previous definitions for PZC and IEP correspond to the whole particle. However, the structural differences on edge and face surfaces, as shown in Figure 2, imply different sensitivities of the edges and faces to protonation and complexation. Therefore, different isoelectric points for edges and faces can be distinguished. The edge isoelectric point is inferred from the formation of expected face-to-edge interparticle associations. The face isoelectric point is very similar to the particle IEP and is also determined using electrophoretic techniques. Clearly, sites with negative and positive charges may coexist on a surface near its isoelectric point.

Dissolution. The stability of minerals in a fluid depends strongly on the characteristics of the fluid, including pH, ionic concentration, type of ion, and temperature. At low pH, the dissolution of clay minerals occurs due to the protonation of OH⁻ and O²⁻ termination sites. Consider the octahedral gibbsite layer, Al(OH)₃. The first, step involves the protonation of two OH⁻ ions to form H₂O and the protonation of nearby O²⁻ in the contiguous Si-tetrahedral layer to form OH⁻. These reactions weaken the bonds that hold the aluminum, resulting in its detachment from the lattice into the aqueous phase as Al³⁺. At this point, the bonds of the silica SiO₂ are weakened, silicon reacts with water, and it is released into the solution as silicic acid, H₄SiO₄. Figure 4 is a schematic representation of the dissolution of the edge of a kaolinite particle. The dissolution reaction for the protonation of kaolinite Al₂Si₂O₅(OH)₄ is (Wieland and Stumm, 1992)



Silicate dissolution in solutions with $\text{pH} > 8$ arises due to the deprotonation of Si-OH sites, according to the following reaction



This reaction weakens adjacent Si-O bonds, thereby releasing Si into solution. In the case of aluminosilicates, it appears that the release of silica governs the detachment of non-silica complexes at high pH

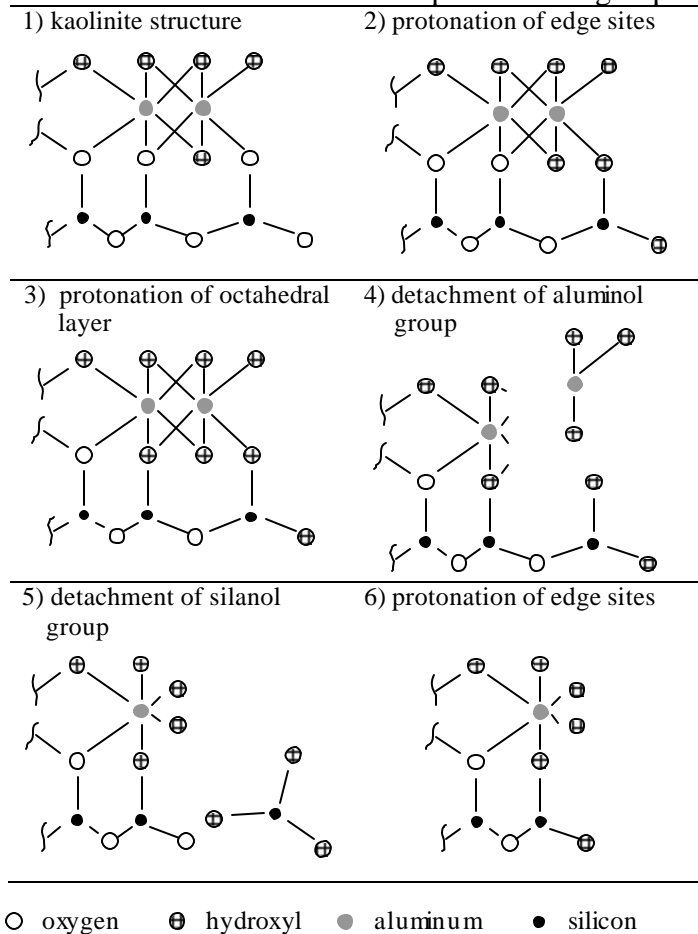


Figure 4. Mechanisms of kaolinite dissolution in acidic solutions (after Wieland and Stumm, 1992).

(Brady and Walther, 1989). This rate-limiting silica dissolution reaction is

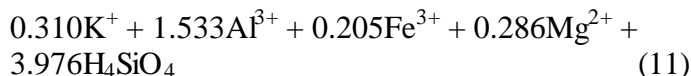


where $\text{Si-O}^- \cdot n\text{H}_2\text{O}$ is the activated complex and n is the number of water molecules. Thus, as pH increases, the concentration of Si-O^- increases (see Equation 9), and the reaction rate increases.

The stability of gibbsite, silica and kaolinite are plotted in Figure 5. Precipitation occurs when ions in the fluid are present at concentrations greater than the stability value; dissolution takes place in the opposite case.

Similar mechanisms occur in the dissolution of montmorillonite. At low pH , the overall dissolution

reaction for a K-montmorillonite is (Furer et al., 1993)



Clearly, gibbsite or silica may reprecipitate after dissolution. Furthermore, the presence of other species renders other effects. For example, the stability curve for iron is very low, hence, even small concentrations of iron in solution tend to precipitate on mineral surfaces altering surface charge density and behavior (e.g., Georgia red clay results from the precipitation of goethite on kaolinite). Finally, dissolution rates are pH dependent.

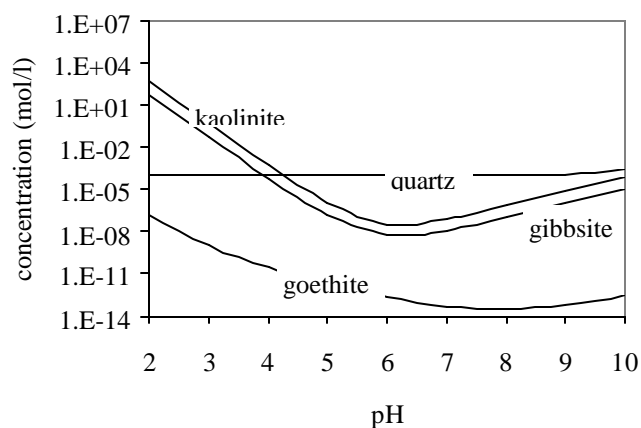


Figure 5. Dissolution - Stability diagram. The concentration of specific ions is used to monitor the evolution of dissolution. (a) Kaolinite dissolution in a 10^{-4} mol/L H_4SiO_4 solution which is typical in fresh, river water (monitored: aluminum). (b) Gibbsite dissolution in water (monitored: aluminum). (c) Quartz dissolution in water (monitored: silicon). (d) Goethite dissolution in water (monitored: iron). Stability constants used to compute this plot are found in Drever (1997).

The dissolution of the mineral consumes H^+ at low pH and OH^- at high pH . Therefore, dissolution promotes a change in extreme values of pH towards the stable pH corresponding to the mineral-fluid system. The liberated ions, such as Al^{3+} at low pH , cause the rapid coagulation of suspensions (around $\text{pH} < 2$ and primarily in face-to-face aggregation; Rand et al., 1980).

3.3 Geometric considerations

Coarse-grained platy particles, such as mica flakes, are controlled by gravity during fabric formation, rendering anisotropic fabrics with horizontally aligned particles (in low concentration deposition). However, particle geometry in fine-grained platy particles, such as clay minerals, colludes with elec-

trical forces in the formation of fine-grained soils. Fabric formation in this case is significantly more intricate.

Specific Surface and Total Charge. The specific surface of a square plate with dimensions $L \times L \times h$ is

$$S_a = \frac{2L^2 + 4hL}{hL^2\rho} = \frac{2}{t\rho} \left(1 + 2\frac{h}{L} \right) \quad (12)$$

where ρ is the mass density of the particle. This equation highlights the prevailing effect of particle thickness on specific surface (a layer of a 2:1 montmorillonite has thickness $h=9.6 \text{ \AA}$ and specific surface $S_a=790 \text{ m}^2/\text{g}$). Furthermore, this relationship shows the small contribution of the edge to the total surface when particles have small thickness-to-length ratios: in kaolinite $h/L < 1/20$ and the edge contribution is $< 10\%$, while in montmorillonite $h/L < 1/100$ and the edge contribution is $< 2\%$. Therefore, pH-dependent changes in edge charge have almost no effect on the charge of montmorillonite particles, and just a minor effect on kaolinite. In other words, the IEP values for the face and for the entire particle are indistinguishable in particles with high slenderness.

Edge and Face Double Layers. Figure 2 shows a schematic cross-section of a kaolinite and a montmorillonite particle with their respective double layers, for average parameters. The visual impact of this figure highlights (1) the increasing relevance of the double layer with decreasing particle length and thickness, and (2) the masking of the edge potential by the face double layer for thin particles. Secor and Radke, (1985) numerically determined the electrostatic potential around a montmorillonite particle. Their results show that the impact of the face potential on the effective edge potential increases as concentration decreases (double layer thickness increases), the ratio of the edge charge density to face charge density decreases, and the ratio of the particle length to thickness increases (Additional corroborating results can be found in Delville, 2001).

3.4 Particle-particle interactions - Multiple scales

The association of two particles reflects the governing interparticle forces. Three minimum energy particle associations are commonly recognized (van Olphen, 1977): Edge-to-Face (EF), Edge-to-Edge (EE) and Face-to-Face (FF). A fourth association, herein called Shifted FF, is frequently observed in SEM pictures (Figure 6). Interparticle forces that promote these associations follow.

Edge-to-Face "flocculation" results from the Coulombian attraction between a positive edge and a

negative face (Schofield and Samson, 1954). EF flocculation can be readily observed in some suspensions at low ionic concentration when the pH is gradually decreased causing a sudden change from a stable suspension (deflocculated- dispersed particles) into a shear resistant mixture; the transition pH marks the edge IEP. Detection is based on indirect parameters, such as the Bingham yield stress, and formed fabrics can be corroborated with SEM pictures when resolution permits. Edge-to-face flocculation is well established in thick particles, such as kaolinite. On the other hand, edge-to-face association is not apparent in montmorillonite (Rand et al., 1980); this may be due to the overwhelming impact of the face double layer on the edge potential as discussed previously in reference to Figure 2.

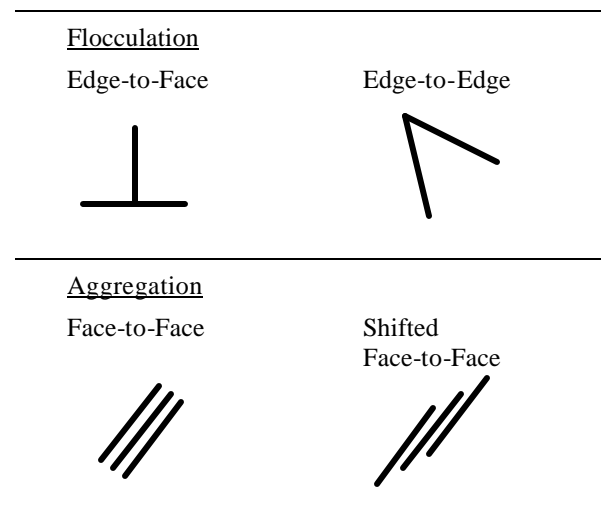


Figure 6. Particle associations. Optimal associations correspond to minimum energy configurations (after van Olphen, 1977).

Face-to-Face "aggregations". Two surfaces (edge or face) with the same charge are subjected to osmotic repulsion and van der Waals attraction. The van der Waals attraction depends on the permittivity of the fluid between the particles (Hamaker constant), which is little affected by ionic concentration. Yet, increasing the ionic concentration reduces the Stern potential (weakening the edge-to-face attraction) and shrinks the double layer thickness or Debye-Hückel length. The net force between two particles as a function of interparticle distance is plotted in Figure 7 for different ionic concentrations. It can be concluded that at low concentrations, osmotic repulsion prevents particle association. On the other hand, osmotic repulsion vanishes at very high concentrations and van der Waals forces prevail.

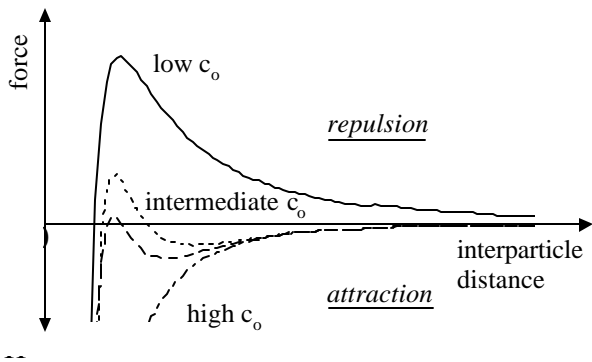


Figure 7. Long-range interparticle force - DLVO Theory. It combines van der Waals attraction (slightly sensitive to c_0) and double layer repulsion (determined by c_0).

Interparticle repulsion can also be overcome by protonation. Indeed, the Stern potential (or the ζ -potential) is zero near the PZC (or the IEP) and there is no interparticle repulsion at distances greater than $\sim 10 \text{ \AA}$.

Particle association by prevailing van der Waals attraction tends to favour face-to-face "aggregation". This association is confirmed by experimental evidence, including the higher density of aggregations. If faces are negative and edges are positive, the minimum energy aggregation is in the form of *shifted face-to-face* association.

Edge-to-Edge "flocculation" is an intermediate condition between EF flocculation and FF aggregation. It is determined by prevailing van der Waals attraction, and it develops at intermediate concentrations, where edge-to-face Coulombian attraction and face-to-face repulsion decrease (van Olphen, 1951).

Groups of associated particles form conglomerates, which in turn form sediments. Therefore, at least three internal scales can be identified: the scale of the particle, the scale of conglomerates, and the scale of the soil mass relevant to the application of interest (Bennett and Hulbert, 1986). Conglomerates bring a new internal scale to soils. For example, FF-aggregated particles may link by the edges to form an "EE-flocculated-aggregated" conglomerate (van Olphen, 1977). The density and mechanical properties of sediments reflect the type of interparticle associations. FF aggregations favor high-density flocs. EF flocs experience both Coulombian and van der Waals attraction forces; this strong particle-particle association has a clear impact on the mechanical properties of sediments.

The rate of particle flocculation or aggregation decreases as solids content decreases, since there are fewer particles available for interactions (Farley and Morel, 1986). The repulsive barrier between particles at intermediate ionic concentrations (Figure 7) also affects the rate of aggregation. Diffusion limited

aggregation occurs when there are negligible repulsive forces between particles, and the rate of aggregation is determined by the rate of particle diffusion due to Brownian motion. Reaction limited aggregation takes place when repulsive forces exist and must be overcome by thermal activation (i.e., agitation). Reaction limited aggregation occurs at a slower rate than diffusion limited aggregation (Lin et al., 1989).

3.5 Fabric formation in the pH-concentration space

The intricate phenomenology outlined above defines particle association and fabric formation as a function of pH and ionic concentration. Figure 8 is an attempt to synthesize these interactions. Due to differences in size and mineralogy, the expected behaviors of kaolinite (Figure 8a) and montmorillonite (Figure 8b) are summarized in separate plots. Boundaries between the different regions coincide with the edge-IEP and the face-IEP (taken as the particle IEP); published values are not consistent, in part due to the interplay between protonation and complexation. Best estimates are used and the c_0 -pH interaction is captured in the curvature of boundary lines.

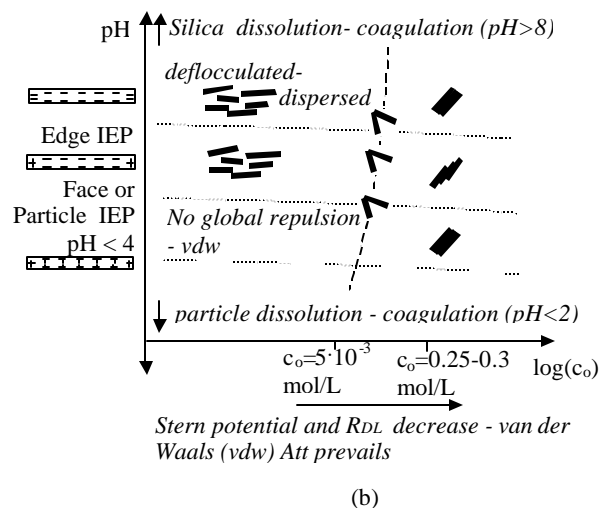
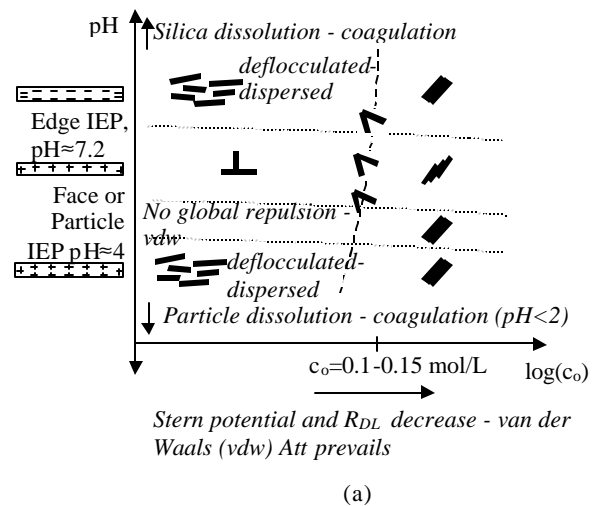


Figure 8. Summary of postulated particle associations (preferred minimum energy configurations) for (a) kaolinite and (b) montmorillonite.

Kaolinite (Figure 8a). At high ionic concentrations, van der Waals forces dominate, and face-to-face aggregation occurs; in NaCl electrolytes, this takes place at concentrations greater than 0.1 to 0.15 mol/L. These aggregates link through edge-to-edge and edge-to-face interactions resulting in a high void ratio network of kaolinite particles (van Olphen, 1977; Rand and Melton, 1977; Melton and Rand, 1977; O'Brien, 1971). At low ionic concentration and high pH, the edge and face are both negatively charged and the double layer is large, thus, clay particles are deflocculated-dispersed. Edge-to-face flocculation is favored due to electrostatic attraction at low ionic concentration and pH less than the edge IEP (pH~7.2) and greater than the particle IEP (i.e., edge positively charged, face negatively charged). For pH<8.5, as ionic concentration increases, edge-to-edge flocs develop. As the pH approaches the particle IEP, the exposed octahedral gibbsite face is positively charged, while the exposed tetrahedral Si-face is negatively charged; while FF aggregation by Coulombian attraction would be expected, this configuration seems improbable, and it appears that EF and EE associations still develop (Rand and Melton, 1977). A deflocculated-dispersed structure is expected at very low pH where the edge and face are both positively charged. At extreme pH, dissolution takes place followed by coagulation.

Montmorillonite (Figure 8b). In general, the effects of ionic concentration and fluid pH on interactions between montmorillonite particles are similar to those in kaolinite, however, the transitions between various fabrics occur at different ionic concentrations and pH. In montmorillonite suspensions with pH between 4 and 11, EE flocculation occurs at NaCl concentrations greater than $5 \cdot 10^{-3}$ mol/L, and FF aggregation occurs at NaCl concentrations greater than 0.25 - 0.3 mol/L (Rand et al., 1980; Chen et al., 1990). The development of EF flocculation in montmorillonite suspensions remains unsettled. Rand et al. (1980) suggested that EF flocculation between montmorillonite particles does not develop at pH between 4 and 11, and some authors believe that EF flocculation does not arise at any pH due to the dominance of the face double layer (Chen et al., 1990). However, Brandenburg and Lagaly (1988) suggested that EF flocculation manifests at pH less than 4. Once again, dissolution is expected at extreme pH values.

It is important to highlight that these maps remain as working hypotheses. The intent is to create a framework to guide further work and to facilitate the interpretation of experimental results. Finally, it is

worth noting that two contiguous particles composed of different minerals may experience strong attraction within the pH range where one particle is negatively charged and the other is positively charged.

4 MACROSCALE OBSERVATIONS AND IMPLICATIONS

The previous discussions suggest that interparticle forces, fabric formation and fabric change can be used to explain chemical-mechanical coupling. Published studies related to variations in the mechanical properties of soils in relation to changes in pore fluid chemistry are summarized in Appendix A. The following observations can be made:

- Many trends appear to be the immediate consequence of changes in double layer thickness ϑ : as the double layer thickness increases, interparticle repulsion forces and porosity increase. This is particularly the case in high specific surface montmorillonite: as ϑ increases, the sedimentation volume and the liquid limit increase; and when ϑ decreases, compressibility decreases and shear wave velocity and shear strength increase.
- Deviations are more common in kaolinite than in montmorillonite, especially when changes in permittivity are involved (the Hamaker constant in the van der Waals force depends on permittivity)

4.1 Counterexamples - Hypotheses

Several salient examples fail to be explained by standard particle-level hypotheses that emphasize the repulsion force. These include: (1) the increase in sedimentation volume with increasing pore fluid ionic concentration, (2) the decrease in small-strain shear stiffness and/or in strength after an increase in pore fluid concentration, and (3) the increase in hydraulic conductivity even though pore fluid changes cause an increase in double layer thickness. The following hypotheses can be considered to explain these deviations:

- Decrease in torsional stability in edge-to-face associations when the ionic concentration increases (M. Geilikman – personal communication). Interparticle force change, so that a two particle aggregation overcomes the repulsion barrier in the interparticle force-distance interaction. Non-monotonic change in interparticle forces within the regime of the cyclic hydration forces (stochastic averaging across the soil mass should conceal this effect).
- Change in fabric (refer to Figure 8).
- Multiple internal scales. The transmission of force in a granular medium takes place along an internal tree-like structure of particles that carry

most of the load (Figure 9). Particles in between these force chains carry small loads, but prevent the highly loaded chains of particles from buckling. Shrinkage between these secondary particles is larger than along the chains because of the lower initial stress (Equation 5), therefore, the stability of the main force chains decreases. This mechanism can explain significant chemical-mechanical coupling effects in soils subjected to fairly high stresses, as long as coupling can alter those weakly loaded particles that act as stabilizing buttresses.

- Development of heterogeneity, with sufficiently soft zones so that the effective medium is less stiff, eventually causing stress concentration and localization.
- The chemical-mechanical history must be carefully taken into consideration. In particular, it is important to establish whether stress-controlled or strain-controlled boundary conditions were maintained. Retraction and fracture formation can take place; for example, when a high concentration pore fluid permeates a soil subjected to zero-strain boundary condition. In this case, potentially high increases in hydraulic conductivity may be observed.

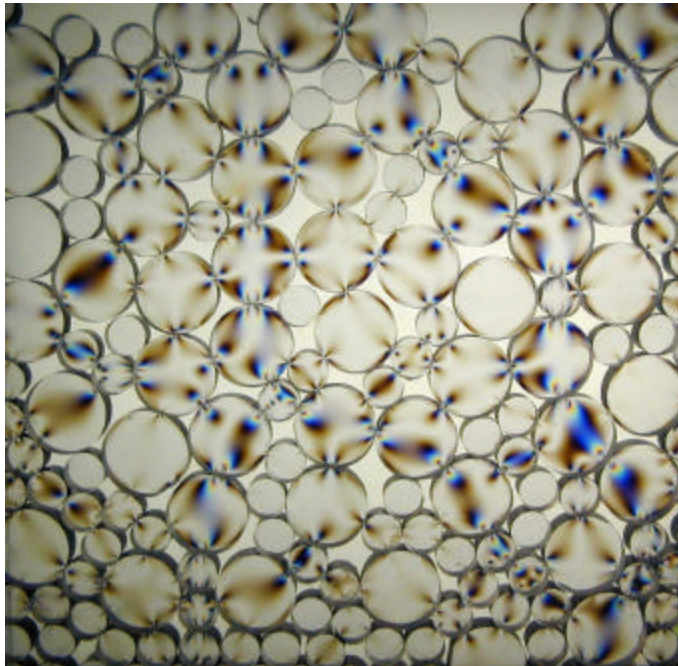


Figure 9. Internal scales. Particles along force-chains carry most of the load. Particles in between these force chains carry small loads but prevent the highly loaded chains of particles from buckling. Shrinkage between these secondary particles

due changes in interparticle forces reduces the stability of the main chains.

Overall, and following the previous discussion on interparticle forces and fabric formation, experimental results must be carefully assessed in terms of initial and final pore fluid conditions and applied state of stress.

4.2 Complexity in chemical-mechanical coupling

The diffusion of a high concentration ionic front tends to promote volume contraction. In turn, this implies the transfer of skeletal load onto the pore fluid, and the generation of a pore pressure front that may even propagate ahead of the ionic front that caused it. Data presented in Figure 10 capture this effect (note the earlier osmotic suction). In soft soils, the amplitude of the pressure front may be on the order of the applied confinement.

4.3 Discussion of modified effective stress definitions

Several heuristic modifications of Terzaghi's effective stress for soils have been proposed to account for local contact-level electrical forces. Both series and parallel models have been assumed (see review in Hueckel, 1992):

$$\sigma' = \sigma - u = R_{DL} - Att \quad \text{Series Model} \quad (13)$$

$$\sigma' = \sigma_{tot} - u - (R_{DL} - Att) \quad \text{Parallel Model} \quad (14)$$

In the series model, an increase in applied stress must be opposed by an increase in repulsion to maintain equilibrium. This model is most applicable to describe volumetric strains for parallel particle packings (face-to-face aggregations) or for very fine soils, such as montmorillonite. The increase in shear strength with normal stress in the series model is attributed to the increase in the viscosity of water between particles (Allam and Sridharan, 1984, argue that viscosity alone cannot explain the measured shear strength). Changes in shear strength due to changes in pore fluid characteristics at constant confinement are readily explained with the parallel model. At the macroscale, the behavior of most clays appears to resemble some combination of both series and parallel models.

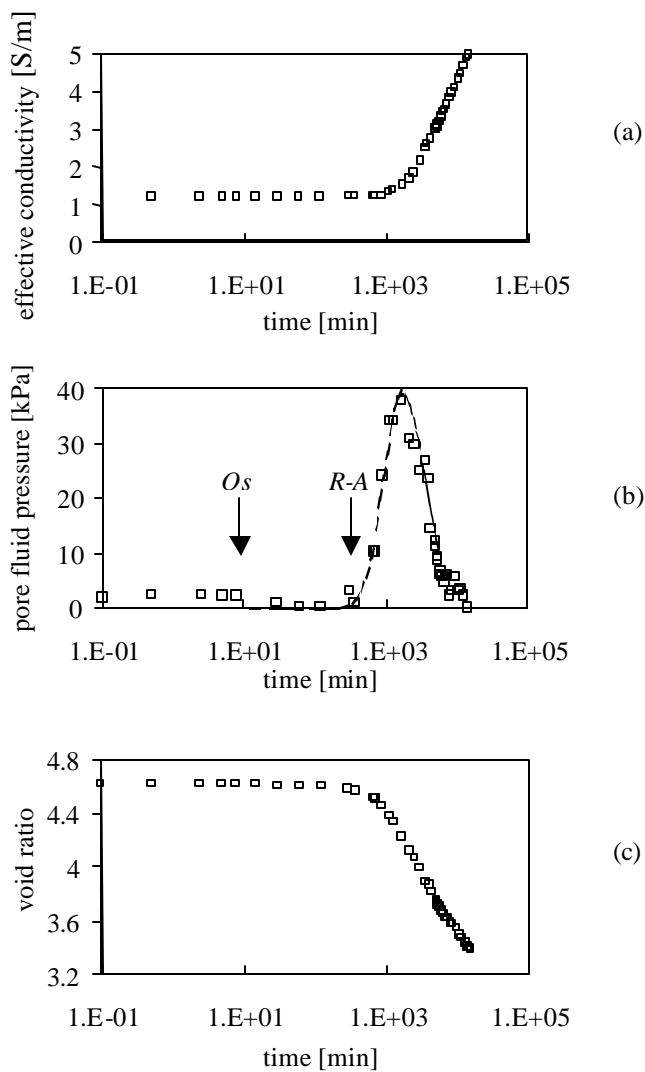


Figure 10. Chemical-mechanical energy coupling. Measured changes in a bentonite specimen subjected to $\sigma'_v=100$ kPa during the diffusion of potassium chloride KCl: (a) effective electrical conductivity (1.3 GHz), (b) pore fluid pressure denouncing the osmotic suction caused at the upper boundary and the subsequent generation of pore pressure associated to osmotic consolidation, and (c) average void ratio (study presented in Santamarina and Fam, 1995 - replotted data).

While these relations may be convenient for many engineering applications, modified effective stress relations often fail to predict observed phenomena, as shown in the exceptions listed in Appendix A. Indeed, the validity of these relations can be disputed on different grounds. First of all, they involve constitutive soil parameters in a definition of a state of stress. Second, they combine physical processes at different scales, with distinct characteristics and effects, mixing boundary-global conditions (Terzaghi effective stress) with local contact-level conditions.

4.4 Long-term chemical-mechanical effects: diagenesis

In general, the term chemical-mechanical coupling refers to events that occur within relatively short time periods. However, chemical changes throughout long periods of time allow for remarkable changes in fabric, mechanical properties and even mineralogy. Examples include pressure-solution-precipitation, the compaction of granular salt, illitization of montmorillonites, and the formation of residual soils.

4.5 Mechanical-chemical coupling

Symmetry in physical phenomena predicts the existence of the counter coupling effect, that is, chemical changes in a system subjected to mechanical excitation. This is indeed the case. For example, ions around clay particles are displaced from their minimum energy configuration during loading and skeletal straining. In time, those ions diffuse into new minimum potential energy positions. Thixotropy is a salient example (Mitchell, 1960; Díaz-Rodríguez and Santamarina, 1999). It is worth noting that the effects of either chemical-mechanical or mechanical-chemical couplings are not reversible.

4.6 Non-aqueous phase liquids: percolation and capillary forces

Polar fluid molecules (such as water) hydrate ions and support the formation of double layers on mineral surfaces leading to interparticle repulsion forces. The Debye-Hückel length and the interparticle repulsion force decrease with decreasing fluid permittivity (Equations 6 and 3). On the other hand, while the van der Waals attraction force does not depend on ion hydration, it does reflect the change in fluid properties through the Hamaker constant (Equation 2): in general, organic fluids render lower interparticle attraction than water.

When a low permeability, non-miscible organic fluid invades the soil, it displaces the aqueous pore fluid, percolating through the network of interconnected porosity, following the path of largest pore throats, in a fractal pattern. The granular skeleton in the presence of non-miscible mixed fluids experiences the effects of interfacial tension and the generation of capillary forces. The capillary forces between two parallel disks separated at a distance t is

$$\text{Capillary force} \quad F_{\text{cap}} = \frac{\pi T_s}{2 t} d^2 \quad (13)$$

where T_s is the surface tension (for water-air: $T_s=0.0727$ N/m). Once again, t and d can be related to macroscale parameters, such as water content w

and specific surface S_a , through relations presented earlier.

In as much as the change in pore fluid involves a second, non-miscible fluid, then the additional involvement of capillary forces should be considered, shifting the boundary and extending the region of possible chemical-mechanical coupling to lower specific surface coarser soils and higher confining stress levels.

Capillary interparticle forces add to skeletal forces, cause the soil to contract, and increase the stiffness and the strength of the soil (at least when homogeneous internal conditions develop). Even if water remains as a percolating phase, the permeability of the medium to water is reduced. Furthermore, because of the fractal nature of the percolation process, the properties of the medium become specimen size dependent.

4.7 Time scales

The time required for chemical-mechanical phenomena is controlled by internal spatial scales in the material, the global diffusion coefficient of the medium D_{medium} [m^2/s], the hydraulic conductivity of the material k [m/s], the particle level diffusion coefficient D_{particle} , and the rate of chemical reactions k_{chem} . When the chemical change results from chemical diffusion taking place across the medium, given a chemical potential difference at the boundaries, then the time scale for coupling is proportional to the distance between the boundaries H ,

$$t = \frac{H^2}{D_{\text{medium}}} \quad \text{diffusion} \quad (14)$$

On the other hand, the new pore fluid may migrate through the medium in response to a pressure gradient i . In this case, the relevant time scale is

$$t = \frac{H}{k i} \quad \text{hydraulic conduction} \quad (15)$$

When seepage occurs, flow prevails in the larger pores. Thereafter, diffusion is required to reach the smaller porosity (Equation 14 is evaluated for the internal length scale H^* between flow channels). Furthermore, the time scale to affect the double layer around a particle, is estimated using Equation 14 for the length scale $H=d$ and the local diffusion coefficient D_{particle} (where D_{particle} can be as low as 10^{-11} m^2/s for the first adsorbed layer - Skipper, 2001). Finally, when the chemical-mechanical coupling involves chemical reactions at the mineral level (i.e., dissolution), the time scale for the coupling is determined by the rate of the reactions captured in the rate constant k_{chem} ,

$$t = \frac{1}{k_{\text{chem}}} \quad \text{rate of chemical reactions} \quad (17)$$

Note that particle-level time scales and macro-scale time scales in soils can be very different. The steady-state distribution of forces within a particulate medium presumes that equilibrium has been reached at all particles. When equilibrium is not attained at a given particle, the particle displaces and alters the equilibrium of its neighbors. Therefore, short particle-level time scales can involve a much longer time scale to fully manifest at the level of the soil mass due to the large number of particles that are recursively involved.

5 CONCLUSIONS

- Fundamental energy principles indicate that energy is coupled in its multiple forms.
- The internal mechanisms that support energy coupling in soils can be complex. They involve changes in interparticle forces, changes in fabric, and interactions among internal scales. Thus, chemical-mechanical coupling may often lead to unforeseen results.
- The potential of chemical-mechanical coupling is greatest in fine-grained soils (e.g. clay minerals) at low confinement.
- Mineralogy and pore fluid determine the chemical-electrical characteristics of mineral surfaces, the ensuing interparticle electrical forces, and fabric formation and its potential alteration during pore fluid changes. Therefore, a detailed analysis of chemical-mechanical coupling must take into consideration changes in surface charge density and double layer formation, the geometric characteristics of the particles, the characteristics of the pore fluid (pH, concentration, ion type), and recognize the interplay between the particle and pore fluid characteristics.
- In its simplest form, fabric formation/alteration in clay minerals can be captured in the pH-concentration space. The resulting fabric formation map is different for different clay minerals, and it may also vary with the valence and size of prevailing ions.
- While heuristically modified effective stress principles are convenient for modeling purposes and can be used to capture some observed results, they are physically ill-posed and fail to predict important aspects of the observed chemical-mechanical coupling response.

6 ACKNOWLEDGMENTS

This study is part of a research program on particulate minerals. Support was provided by the National Science Foundation and the Georgia mining industry.

REFERENCES

- Abdul, A. S., Gibson, T. L. and Rai, D. N., 1990, "Laboratory studies of the flow of some organic solvents and their aqueous solutions through bentonite and kaolin clays", *Ground Water*, vol. 28, no. 4, pp. 524-533.
- Acar, Y. B. and Olivieri, I., 1989, "Pore fluid effects on the fabric and hydraulic conductivity of laboratory-compacted clay", *Transportation Research Records*, vol. 1219, pp. 144-159.
- Allam, M. M. and Sridharan, A., 1984, "The shearing resistance of saturated clays", *Géotechnique*, vol. 34, pp. 119-22.
- Amirtharajah, A. and Mills, K. M., April 1982, "Rapid-mix design for mechanisms of alum coagulation", *American Water Works Association Journal*, pp. 210-216.
- Barbour, S. L., and Yang, N., 1993, "A review of the influence of clay-brine interaction on the geotechnical properties of ca-montmorillonite clayey soils from Western Canada", *Canadian Geotechnical Journal*, vol. 30, pp. 920-934.
- Bennett, R.H. and Hulbert, M.H. (1986), *Clay Microstructure*, International Human Resources Development Corporation, Boston, 161 pages.
- Bowders, J. J. and Daniel, D. E., 1987, "Hydraulic conductivity of compacted clay to dilute organic chemicals", *Journal of Geotechnical Engineering*, vol. 113, no. 12, pp. 1432-1448.
- Bowders, J. J., 1985, "The influence of various concentrations of organic liquids on the hydraulic conductivity of compacted clay", Geotechnical Engineering Dissertation GT85-2, The University of Texas at Austin, 218 p.
- Brady, P.V. and Walther, J.V., 1989, "Controls on silicate dissolution rates in neutral and basic pH solutions at 25°C", *Geochimica et Cosmochimica Acta*, vol. 53, pp. 2823-2830.
- Brandenburg, U. and Lagaly, G., 1988, "Rheological Properties of Sodium Montmorillonite Dispersions", *Applied Clay Science*, Vol. 3, pp. 263-279.
- Chan, P. C., Selvakumar, G., and Shih, C. Y., 1986, "The effects of liquid organic contaminants on geotechnical properties of clay soils", *Proceedings 18th Mid-Atlantic Industrial Waste Conference*, Boardman, G. D. (ed.), pp. 409-420.
- Chen, J. S., Cushman, J. H., and Low, P. F., 1990, "Rheological Behavior of Na-Montmorillonite Suspensions at Low Electrolyte Concentrations", *Clays and Clay Minerals*, Vol. 38, No. 1, pp. 57-62.
- Chen, J., Anandarajah, A., and Inyang, H., 2000, "Pore fluid properties and compressibility of kaolinite", *Journal of Geotechnical and Geoenvironmental Engineering*, vol. 126, no. 9, pp. 798-807.
- Delgado, A., Gonzalez-Caballero, F., and Bruque, J. M., 1986, "On the Zeta Potential and Surface Charge Density of Montmorillonite in Aqueous Electrolyte Solutions", *Journal of Colloid and Interface Science*, vol. 113, no. 1, pp. 203-211.
- Delville, A. (2001), The Influence of Electrostatic Forces on the Stability and the Mechanical Properties of Clay Suspensions, Proc. Workshop on Clay Behaviour: Chemo-Mechanical Coupling, Edts., C. Di Maio, T. Hueckel, and B. Loret, Maratea, Italy, 20p.
- Díaz-Rodríguez, J.A. and Santamarina, J.C. (1999), "Thixotropy: The Case of Mexico City Soils", *XI Panamerican Conf. on Soil Mech. and Geotech. Eng.*, Iguazu Falls, Brazil, vol. 1 pp. 441-448.
- Di Maio C., and Fenelli, G. B., 1994, "Residual strength of kaolin and bentonite: the influence of their constituent pore fluid", *Geotechnique*, vol. 44, no. 4, pp. 217-226.
- Di Maio, C. (1996) Exposure of bentonites to salt solution: osmotic and mechanical effects. *Geotechnique*, vol. 46, no. 4, pp. 695-707.
- Drever, J.I., 1997, *The Geochemistry of Natural Waters*, 3rd Edition, Prentice Hall, Upper Saddle River, NJ, 436p.
- Dunn, R. J., and Mitchell, J. K., 1984, "Fluid conductivity testing of fine grained soils", *Journal of Geotechnical Engineering Division*, ASCE, vol. 110 (GT11), pp.1648-1665.
- Evans, J. C., Fang, H. Y., and Kugelman, I. J., 1985, "Organic fluids effect on the permeability of soil-bentonite slurry walls", *Proceedings National Conference. Hazardous Waste and Environmental Emergencies*, Cincinnati, OH.
- Farley, K. J. and Morel, F. M. M., 1986, "Role of Coagulation in the Kinetics of Sedimentation", *Environmental Science Technology*, vol. 20, no. 2, pp. 187-195.
- Fernandez, F. and Quigley, R. M., 1985, "Hydraulic conductivity of natural clays permeated with simple liquid hydrocarbons", *Canadian Geotechnical Journal*, vol. 22, pp.205-214.
- Furer, G., Zysset, M. and Schindler, P. W., 1993, "Chapter 10: Weathering kinetics of montmorillonite: Investigations in batch and mixed-flow reactors", *Geochemistry of Clay-Pore Fluid Interactions*, The Mineralogical Society Series, Edited by D. Manning, P. Hall and C. Hughes, Chapman & Hall, New York, pp. 243-262.
- Hayes, K. F. and Leckie, J. O., 1987, "Modeling Ionic Strength Effects on Cation Adsorption at Hydrous Oxide/Solution Interfaces", *Journal of Colloid and Interface Science*, vol. 115, no. 2, pp. 564-572.
- Holden, A., 1965, *The Nature of Solids*, Dover Publications, Inc. New York. 241p.
- Hueckel, T. A., 1992. "On the Effective Stress Concepts and Deformation in Clays Subjected to Environmental Loads: Discussion", *Canadian Geotechnical Journal*, vol. 29, pp. 1120-1125.
- Ikeda, T., 1990, *Fundamentals of Piezoelectricity*, Oxford U. Press. Oxford. 263p.
- Kenny, T. C., 1967, "The influence of mineral composition on the residual strength of natural soils", *Proceedings Geotechnical Engineering Conference*, Oslo, vol. 1, pp. 123-129.
- Klein, K., 1999, *Electromagnetic Properties of High Specific Surface Minerals*, Ph.D. Dissertation, Georgia Institute of Technology, Atlanta, 335p.
- Lin, M. Y., Lindsay, H. M., Weitz, D. A., Ball, R. C., Klein, R., and Meakin, P., 1989, Letter: "Universality in colloid aggregation", *Nature*, vol. 339, pp. 360-362.
- Lovgren, L., Sjoberg, S., and Schindler, P. W., 1990, "Acid/base reactions and Al(III) complexation at the surface of goethite", *Geochimica et Cosmochimica Acta*, vol. 54, pp. 1301-1306.
- Lutz, J. F., and Kemper, W. D., 1959, "Intrinsic permeability of clays as affected by clay-water interaction", *Soil Science*, vol. 88, pp. 83-90.
- Lyklema, J., 1995, *Fundamentals of Interface and Colloid Science Volume II: Solid-Liquid Interfaces*, Academic Press, New York.
- Madsen, F. T., and Mitchell, J. K., 1989, "Chemical effects on clay hydraulic conductivity and their determination", No.

- 135, Mitteilungen des Institutes für Grundbau und Bodenmechanik Eidgenössische Technische Hochschule, Zurich, 56p.
- Meegoda, N. J. and Ratnaweera, P., 1994, "Compressibility of contaminated fine-grained soils", *Geotechnical Testing Journal*, vol. 17, no. 1, pp. 101-112.
- Melton, I. E. and Rand, B., 1977, "Particle Interactions in Aqueous Kaolinite Suspensions III. Sedimentation Volume", *Journal of Colloid and Interface Science*, vol. 60, no. 2, pp. 331-336.
- Mesri, G., and Olsen, R. E., 1970, "Shear strength of montmorillonite", *Geotechnique*, vol. 20, no. 3, pp. 261-270.
- Mesri, G., and Olsen, R. E., 1971, "Consolidation characteristics of montmorillonite", *Geotechnique*, vol. 21, no. 4, pp. 341-352.
- Mitchell, J.K., 1960, "Fundamentals Aspects of Thixotropy in Soils". *Journal of the Soil Mechanics and Foundations Division*, ASCE, vol. 86, pp. 19-52.
- Mitchell, J. K., 1993, *Fundamentals of Soil Behavior*, Second Edition, John Wiley & Sons, Inc., New York, 437p.
- Moore, R., 1991, "The chemical and mineralogical controls upon the residual strength of pure and natural clays", *Geotechnique*, vol. 41, no. 1, pp. 35-47.
- Nishimura, S., Tateyama, H., Tsunematsu, K., and Jinnai, K., 1992, "Zeta Potential Measurement of Muscovite Mica Basal Plane-Aqueous Solution Interface by Means of Plane Interface Technique", *Journal of Colloid and Interface Science*, vol. 152, no. 2, pp. 359-367.
- Nishimura, S., Biggs, S., Scales, P. J., Healy, T. W., Tsunematsu, K., and Tateyama, T., 1994, "Molecular-Scale Structure of the Cation Modified Muscovite Mica Basal Plane", *Langmuir*, vol. 10, pp. 4554-4559.
- O'Brien, N. R., 1971, "Fabric of Kaolinite and Illite Flocules", *Clays and Clay Minerals*, vol. 19, pp. 353-359.
- Parks, G.A. (1990), Surface Energy and Adsorption at Mineral/Water Interfaces: An Introduction, in *Mineral-Water Interface Geochemistry*, Eds. M.F. Hochella and A.F. White, vol. 23, Mineralogical Society of America, Washington, pp. 133-175.
- Pierre, A. C., and Ma, K., 1999, "DLVO theory and clay aggregate architectures formed with AlCl₃", *Journal of European Ceramic Society*, vol. 19, no. 8, pp. 1615-1622.
- Quirk, J. P., and Schofield, R. K., 1955, "The effect of electrolyte concentration on soil permeability", *Journal of Soil Science*, vol. 6, no. 2, pp. 163-178.
- Rand, B. and Melton, I. E., 1977, "Particle Interactions in Aqueous Kaolinite Suspensions I. Effect of pH and Electrolyte upon the Mode of Particle Interaction in Homoionic Sodium Kaolinite Suspensions", *Journal of Colloid and Interface Science*, vol. 60, no. 2, pp. 308-320.
- Rand, B., Pekenc, E., Goodwin, J. W., and Smith, R. W., 1980, "Investigation into the Existence of Edge-Face Coagulated Structures in Na-Montmorillonite Suspensions", *Journal of the Chemical Society, Faraday Transaction I*, vol. 76, pp. 225-235.
- Ridley, K. J. D., Bewtra, J. K., and McCorquodale, J. A., 1984, "Behavior of compacted fine-grained soil in a brine environment", *Canadian Journal Geotechnical Engineering*, vol. 11, 196-203.
- Santamarina, J.C., and Fam, M. (1995), Changes in Dielectric Permittivity and Shear Wave Velocity During Concentration Diffusion, *Canadian Geotechnical Journal*, vol. 32, no. 4, 647-659.
- Santamarina, J. C. and Fratta, D., 2001, "Dynamic Electrical-Mechanical Energy Coupling In Electrolyte-Mineral Systems", *Journal of Transport In Porous Media* (Submitted).
- Santamarina, J.C., Klein, K. and Fam, M. (2001). *Soils and Waves*, J. Wiley and Sons, Chichester, UK, 488p.
- Schofield, R. K. and Samson, H. R., 1954, "Flocculation of Kaolinite due to the Attraction of Oppositely Charged Crystal Faces", *Faraday Society Discussions*, no. 18, pp. 135-145.
- Secor, R. B. and Radke, C. J., 1985, "Spillover of the Diffuse Double Layer on Montmorillonite Particles", *Journal of Colloid and Interface Science*, vol. 103, no. 1, pp. 237-244.
- Skipper, N.T. (2001), Influence of Pore-Liquid Composition on Clay Behaviour: Molecular Dynamics Simulations of Nano-Structure, *Proc. Workshop on Clay Behaviour: Chemo-Mechanical Coupling*, Edts., C. Di Maio, T. Hueckel, and B. Loret, Maratea, Italy. 18p.
- Sivapullaiah, P. V., and Sridharan, A., 1987, "Effect of polluted water on the physico-chemical properties of clayey soils", *Environmental Geotechnics and Problematic Soils and Rocks*, Balasubramaniam et al. (eds.), Balkema, Rotterdam, pp. 179-190.
- Sridharan, A., and Prakash, K., 1999, "Influence of clay mineralogy and pore-medium chemistry on clay sediment formation", *Canadian Geotechnical Journal*, vol. 36, pp. 961-966.
- Sridharan, A., and Rao, V. G., 1973, "Mechanisms controlling volume change of saturated clays and the role of effective stress concept", *Geotechnique*, vol. 23, no. 3, pp. 359-382.
- Sridharan, A., and Rao, V. G., 1979, "Shear strength behavior of saturated clays and the role of effective stress concept", *Geotechnique*, vol. 29, no. 2, pp. 177-193.
- Sridharan, A., and Sivapullaiah, P. V., 1987, "Engineering behavior of soils contaminated with different pollutants", *Environmental Geotechnics and Problematic Soils and Rocks*, Balasubramaniam et al. (eds.), Balkema, Rotterdam, pp. 165-178.
- Sridharan, A., 2001, Engineering Behaviour of Clays: Influence of Mineralogy, , *Proc. Workshop on Clay Behaviour: Chemo-Mechanical Coupling*, Edts., C. Di Maio, T. Hueckel, and B. Loret, Maratea, Italy.
- Sposito, G., 1998, "On Points of Zero Charge", *Environmental Science & Technology*, vol. 32, no. 19, pp. 2815-2819.
- Stumm, W., 1992, *Chemistry of the Solid-Water Interface*, John Wiley & Sons, Inc., New York, 428p.
- van Olphen, 1951, "Rheological Phenomena of Clay Sols in Connection with the Charge Distribution on the Micelles", *Discussions of the Faraday Society*, no. 11, pp. 82-84.
- van Olphen, 1977, *Clay Colloid Chemistry*, Second Edition, Krieger Publishing Company, Malabar, Florida, 318p.
- Warkentin, B. P., 1961, "Interpretation of the upper plastic limit of clays", *Nature*, vol. 190, pp. 287-288.
- Weaver, C. E., 1989, *Clays, Muds, and Shales*, Elsevier, New York, 819p.
- Wieland, E. and Stumm, W., 1992, "Dissolution kinetics of kaolinite in acidic solutions at 25°C", *Geochimica et Cosmochimica Acta*, vol. 56, pp. 3339-3355.
- Williams, D. J. A. and Williams, K. P., 1978, "Electrophoresis and Zeta Potential of Kaolinite", *Journal of Colloid and Interface Science*, vol. 65, no. 1, pp. 79-87.
- Yong, R. N., and Warkentin, B. P., 1966, *Introduction to Soil Behavior*, Macmillan Co., New York, 451p.

Appendix A. Differences between kaolinite and montmorillonite (updated after Santamarina and Fam, 1995).

Property	Sample preparation	Observed trends		Reference
		Kaolinite ¹	Montmorillonite ¹	
Hydraulic Conductivity	Hydraulic conductivity was estimated from consolidation tests. Air-dried samples were mixed with ethyl alcohol, centrifuged, dried, and then fluids were added.	$\epsilon' \downarrow \Rightarrow k_p \downarrow^2$	$\epsilon' \downarrow \Rightarrow k_p \uparrow$	Madsen and Mitchell (1989) Mesri and Olsen (1971)
	Samples contained various concentrations of methanol and acetic acid.	methanol $c < 80\%$ $\epsilon' \downarrow \Rightarrow k_p \sim$ $c > 80\%$ $\epsilon' \downarrow \Rightarrow k_p \uparrow$ acetic acid $c < 100\%$ $\epsilon' \downarrow \Rightarrow k_p \downarrow$ $c = 100\%$ $\epsilon' \downarrow \Rightarrow k_p \uparrow$	---	Bowders and Daniel (1987)
	Samples compacted and permeated with different organic fluids. k_p measured using a flexible wall permeameter during fluid exchange.	$\Delta \epsilon' \Rightarrow \Delta k_p$ no clear trend	$\Delta \epsilon' \Rightarrow \Delta k_p$ no clear trend	Acar and Olivieri (1989)
	Kaolinite samples were compacted and bentonite samples were consolidated from slurry. Hydraulic conductivity was measured using a flexible wall permeameter during fluid exchange.	$\epsilon' \downarrow \Rightarrow k_p \downarrow$ or remains constant	$\epsilon' \downarrow \Rightarrow k_p \uparrow$	Bowders (1985) Evans et al. (1985) (both references from Madsen and Mitchell, 1989)
	Natural clayey soil mixed with fluids of varying dielectric permittivity.	clay minerals: ~50% illite, ~15% smectite $\epsilon' \downarrow \Rightarrow k_p \uparrow$ (for constant void ratio)		Fernandez and Quigley (1985)
	Water-compact natural clayey soil, permeated with various concentrations of ethanol and dioxane. Confining stress approximately zero.	clay minerals: ~50% illite, ~15% smectite ethanol $c < 60\%$, dioxane $c < 70\%$ $\epsilon' \downarrow \Rightarrow k_p \downarrow$ ethanol $c > 70\%$, dioxane $c > 70\%$ $\epsilon' \downarrow \Rightarrow k_p \uparrow$		Fernandez and Quigley (1985)
	Water saturated clays ($c=0.005$ N calcium sulfate) permeated with organic fluids at different c .	$c < 50\%$ $\epsilon' \downarrow \Rightarrow k_p \sim$ $c = 100\%$ $\epsilon' \downarrow \Rightarrow k_p \uparrow$	$c = 10\%$ $\epsilon' \downarrow \Rightarrow k_p \downarrow$ $c = 100\%$ $\epsilon' \downarrow \Rightarrow k_p \uparrow$	Abdul et al. (1990)
	Na-, Ca- and H-clays were tested. The percolating fluids were water, NaCl, CaCl ₂ and HCl at concentrations 0.005 N and 0.5 N).	$c \uparrow \Rightarrow k_p \uparrow$	$c \uparrow \Rightarrow k_p \uparrow$	Lutz and Kemper (1959)
	Compacted samples were soaked in high concentration NaCl brine for one year.	$c \uparrow \Rightarrow k_p \uparrow$	$c \uparrow \Rightarrow k_p \uparrow$	Ridley et al. (1984)
	Homoionic samples prepared by repeated washing the clay with 1 N solution of the required ion. The excess solution was removed by distilled water.	$c \uparrow \Rightarrow k_p \uparrow$	$c \uparrow \Rightarrow k_p \uparrow$	Mesri and Olsen (1971) Dunn and Mitchell (1984) Quirk and Schofield (1955)
Sedimentation	Samples were prepared by mixing dry clay with water and carbon tetrachloride, respectively.	$\epsilon' \uparrow \Rightarrow e \downarrow$	$\epsilon' \uparrow \Rightarrow e \uparrow$	This study
	Samples mixed with water. Salt was added after hydration. After vigorous mixing, they were allowed to settle.	$c \uparrow \Rightarrow e \downarrow$ $z \uparrow \Rightarrow e \downarrow$	$c \uparrow \Rightarrow e \downarrow$ $z \uparrow \Rightarrow e \downarrow$	This study
	Soils were converted to Na-clays. Various concentrations of AlCl ₃ were added ($c < 50$ mmol/L). A dispersant was added to the sedimentation columns (Na ₄ P ₂ O ₇).	$c < 0.2$ mmol/L, pH < 9.4 $c \uparrow \Rightarrow e \uparrow$ $c > 0.2$ mmol/L, pH < 9.4 $c \uparrow \Rightarrow e \downarrow$	$c < 3-5$ mmol/L, pH < 9.5 $c \uparrow \Rightarrow e \uparrow$ 3-5 < $c < 10$ mmol/L, pH < 9.5 $c \uparrow \Rightarrow e \downarrow$	Pierre and Ma (1999)
	Samples were placed in solutions with different organic fluids, different NaCl concentrations, and various chlorides (K, NH ₄ , Na, Li, Ba, Ca, Mg).	$\epsilon' \uparrow \Rightarrow e \downarrow$ $c \uparrow \Rightarrow e \uparrow$ $z \uparrow \Rightarrow e$ no trend	$\epsilon' \uparrow \Rightarrow e \uparrow$ $c \uparrow \Rightarrow e \downarrow$ $z \uparrow \Rightarrow e$ no trend	Sridharan and Prakash (1999)

Liquid Limit	Samples mixed with different organic fluids. Liquid limit was determined using cone test, and reported in terms of volumetric water content to avoid the effect of the variable unit weight of the fluids.	$\epsilon' \uparrow \Rightarrow LL \downarrow$ Not monotonic	$\epsilon' \uparrow \Rightarrow LL \uparrow$	Sivapullaiah and Sridharan (1987) This study
	Samples mixed with different organic fluids.	$\epsilon' \uparrow \Rightarrow LL$ no trend	$\epsilon' \uparrow \Rightarrow LL \uparrow$	Acar and Olivieri (1989)
	Mixed with various concentrations of propanol (12.5-50%) and glycerol (16.5-44%) in a NaCl solut.	$\epsilon' \uparrow \Rightarrow LL \downarrow$	---	Meegoda and Ratnaweera (1994)
	Samples were mixed with various concentrations of methanol and acetic acid. Samples were also prepared at one concentration for heptane and TCE.	$\epsilon' \uparrow \Rightarrow LL \downarrow$	---	Bowders and Daniel (1987)
	Mixed with different concentrations of phenol (10^{-10^5} $\mu\text{g/L}$).	$c \uparrow \Rightarrow \epsilon' \downarrow \Rightarrow LL \uparrow$	---	Chan et al. (1986)
	Samples were mixed with aqueous solutions of different valence ions at varying concentrations. (Note: contradictory data in Sridharan 2001)	$c \uparrow \Rightarrow LL \downarrow^3$ $LL_{Ca} > LL_{Na}$	$c \uparrow \Rightarrow LL \downarrow$ $LL_{Ca} < LL_{Na}$	Mesri and Olsen (1970) Yong and Warkentin (1966) This study
	Samples soaked in high concentration NaCl brine	$c \uparrow \Rightarrow LL \downarrow$	$c \uparrow \Rightarrow LL \downarrow$	Ridley et al. (1984)
	Samples were mixed with different organic fluids and then consolidated.	$\epsilon' \uparrow \Rightarrow e \downarrow$	$\epsilon' \uparrow \Rightarrow e \uparrow$	Sridharan and Sivapullaiah (1987)
Consolidation	Clays were mixed with carbon tetrachloride, consolidated, and then water was added at 12.5 kPa.	$\epsilon' \uparrow \Rightarrow e \downarrow$	$\epsilon' \uparrow \Rightarrow e \uparrow$	Sridharan and Rao (1973)
	Mixed with various concentrations of propanol (12.5-50%) and glycerol (16.5-44%) in NaCl solution. Applied stress from 25kPa to 1600kPa.	$\epsilon' \uparrow \Rightarrow e \uparrow$	---	Meegoda and Ratnaweera (1994)
	Samples were mixed with fluids with different permittivities (nine organic fluids) and then consolidated under stresses from 0-300 kPa.	$\epsilon' < \sim 30$ and $\epsilon' > \sim 80$ $\epsilon' \uparrow \Rightarrow e \downarrow$ $\sim 30 < \epsilon' < \sim 80$ $\epsilon' \uparrow \Rightarrow e \uparrow$	---	Chen et al. (2000)
	Samples were prepared using the slurry technique. They were consolidated to 105 kPa in an isotropic cell before adding KCl solution (4.0 M).	$c \uparrow \Rightarrow e \downarrow^4$	$c \uparrow \Rightarrow e \downarrow$	Santamarina and Fam (1995)
	Samples were prepared using the slurry technique. They were consolidated to 105 kPa in an isotropic cell before adding KCl solution (4.0 M).	$c \uparrow \Rightarrow V_s \downarrow$	$c \uparrow \Rightarrow V_s \uparrow$	Santamarina and Fam (1995)
Shear Strength	Oven dried samples were statically compacted inside the direct shear box, and loaded to the desired stress. Samples were flooded with different organic fluids. Finally shear was applied.	$\epsilon' \downarrow \Rightarrow C^* \uparrow$ $\epsilon' \downarrow \Rightarrow \phi \uparrow$	$\epsilon' \downarrow \Rightarrow C^* \uparrow$ $\epsilon' \downarrow \Rightarrow \phi \uparrow$	Sridharan and Rao (1979)
	Homoionic samples were prepared as described under hydraulic conductivity (the effect of concentration change decreased for higher confining pressure). Shear box or ring shear devices were used.	Not monotonic	$c \downarrow \Rightarrow C^* \uparrow$ $c \downarrow \Rightarrow \phi \uparrow$	Mesri and Olsen (1970) Kenny (1967) Moore (1991) Di Maio and Fenelli (1994)

The characteristics of kaolinite and bentonite vary among authors. In all cases, kaolinite has low specific surface, whereas, montmorillonite has high specific surface.

Contradictory data were also reported by Madsen and Mitchell (1989).

At pH = 10, the liquid limit increases with concentration (Warkentin, 1961).

If permeate is of lower concentration, early collapse may take place followed by swelling (Barbour and Yang, 1993).

Variables: ϵ' dielectric permittivity; $\Delta\epsilon'$ change in the permittivity of pore fluid; c concentration; Δc change in concentration of the pore water; cation valence.

Parameters: k_p hydraulic conductivity; LL liquid limit; e void ratio; V_s shear wave velocity; C^* shear intercept; ϕ angle of shearing resistance.